Research Article

Haoran Zhang, Tao Wang*, Jingyi Tian, Jiacheng Sun, Shaoxian Li, Israel De Leon, Remo Proietti Zaccaria, Liang Peng, Fei Gao, Xiao Lin, Hongsheng Chen* and Gaofeng Wang*

Quasi-BIC laser enabled by high-contrast grating resonator for gas detection

https://doi.org/10.1515/nanoph-2021-0368
Received July 12, 2021; accepted November 21, 2021;
published online December 1, 2021

Abstract: In this work, we propose and numerically investigate a two-dimensional microlaser based on the concept of bound states in the continuum (BIC). The device consists of a thin gain layer (Rhodamine 6G dye-doped silica) sandwiched between two high-contrast-grating layers. The structure supports various BIC modes upon a proper choice of topological parameters; in particular it supports a high-Q quasi-BIC mode when partially breaking a bound state in the continuum at Γ point. The optically-pumped gain medium provides sufficient optical gain to compensate the quasi-BIC mode losses, enabling lasing with ultra-low pump threshold (fluence of 17 $\mu J/cm^2$) and very narrow optical linewidth in the visible range. This innovative device displays distinguished sensing performance for gas detection, and the emission wavelength sensitively shifts to the longer wavelength with the changing of environment refractive index (in order of 5×10^{-4}). The achieved bulk sensitivity is 221 nm/RIU with a high signal to noise ratio, and a record-high figure of merit reaches to 4420 RIU^{-1}. This ultracompact and low threshold quasi-BIC laser facilitated by the ultra-narrow resonance can serve as formidable candidate for on-chip gas sensor.

***Corresponding authors**: **Tao Wang**, Engineering Research Center of Smart Microsensors and Microsystems of MOE; and School of Electronics and Information, Hangzhou Dianzi University, Hangzhou, 310018, China, E-mail: wangtao@hdu.edu.cn. https://orcid.org/0000-0003-3322-7554; **Hongsheng Chen**, Interdisciplinary Center for Quantum Information, College of Information Science and Electronic Engineering, Zhejiang University, Hangzhou 310027, China, E-mail: hansomchen@zju.edu.cn. https://orcid.org/0000-0002-5735-9781; and **Gaofeng Wang**, Engineering Research Center of Smart Microsensors and Microsystems of MOE; and School of Electronics and Information, Hangzhou Dianzi University, Hangzhou, 310018, China, E-mail: gaofeng@hdu.edu.cn. https://orcid.org/0000-0001-8599-7249

Haoran Zhang and Shaoxian Li, Engineering Research Center of Smart Microsensors and Microsystems of MOE; and School of Electronics and Information, Hangzhou Dianzi University, Hangzhou, 310018, China, E-mail: 192040228@hdu.edu.cn (H. Zhang), lishaoxian@hdu.edu.cn (S. Li)

Liang Peng, School of Information and Electrical Engineering, Zhejiang University City College, Hangzhou, 310015, China, E-mail: pengl@zucc.edu.cn

Jingyi Tian, Centre for Disruptive Photonic Technologies, TPI, SPMS, Nanyang Technological University, Nanyang, 637371, Singapore, E-mail: jingyi.tian@ntu.edu.sg

Jiacheng Sun, Engineering Research Center of Smart Microsensors and Microsystems of MOE; and School of Zhuoyue Honors, Hangzhou Dianzi University, Hangzhou, 310018, China, E-mail: jiacheng_jason_sun@hdu.edu.cn

Israel De Leon, School of Engineering and Sciences, Tecnológico de Monterrey, Monterrey, Nuevo León 64849, Mexico, E-mail: ideleon@tec.mx

Remo Proietti Zaccaria, Cixi Institute of Biomedical Engineering, Ningbo Institute of Materials Technology and Engineering, Chinese Academy of Sciences; Italian Institute of Technology, via Morego 30, 16163 Genova, Italy, E-mail: remo.proietti@iit.it

Fei Gao and Xiao Lin, Interdisciplinary Center for Quantum Information, College of Information Science and Electronic Engineering, Zhejiang University, Hangzhou 310027, China, E-mail: gaofeizju@zju.edu.cn (F. Gao), xiaolinzju@zju.edu.cn (X. Lin)

1 Introduction

In recent years, the investigation of bound states in the continuum (BICs) has attracted substantial attention due to the interesting physics and practical applications [1]. The BIC theory originated from quantum mechanics and was firstly proposed by von Neumann and Wigner in 1929 [2, 3]. Since then, it has been used to explain the important physical concept of resonance with infinite lifetime in various physical systems, such as photonics [4–7], acoustics [8, 9] and water waves [10]. According to Neumann and Wigner's seminal work [2], when two resonances pass each other as a function of a continuous parameter, the two channels will interfere, and give rise to an avoided crossing for their resonances. Theoretically, at a given value of the continuous parameter, one of the channels vanishes entirely and hence becomes a dark mode (BIC mode) with an infinite quality (Q) factor [11]. In practice, BICs are limited by finite structure size, material

absorption, and structural imperfection [12], they manifest themselves and collapse to Fano resonant states with long lifetime, also known as quasi-BICs [13, 14]. Recently, high-Q quasi-BICs have been observed in many passive systems, and it has been recognized that practical systems supporting such resonances are well suited for lasing and sensing applications [15, 16].

Sub-wavelength high-contrast gratings (HCGs) possess distinct features, such as broadband high reflectivity ($> 99\%$) and high-Q resonances ($> 10^7$) [17]. In particular, it has been shown that HCG systems can support BICs with improved spectral performance [1, 18]. The narrow spectral linewidth (γ) featured by these structures are very sensitive to changes in refractive index around them [19], making them promising candidates for engineering optical sensors with high sensitivity (S) and excellent figure of merit, FOM $= S/\gamma$ [20]. However, investigations thus far have considered only passive structures, which can limit significantly the device's sensitivity [21]. Recent studies indicate that active sensors based on small lasers not only supply coherent radiation, but also show enhanced sensing performance [22, 23]. Thus, photonic structures supporting high-Q quasi-BIC lasers are of great interest in sensing applications, as they could offer possibilities of achieving a sensing performance beyond that of more conventional photonic sensors [24, 25].

Lasing action based on BICs or quasi-BICs in two-dimensional photonic-crystal structures has been reported recently [15, 16, 26]. Nonetheless, investigations on potential applications of such devices are scarce, e.g., active sensing based on BIC lasers. In this work, we propose an innovative resonator composed of highly reflecting HCG layers surrounding a thin organic-dye-doped SiO_2 layer working as gain material for laser emission. This ultracompact resonator design not only opens an alternative route to generate different resonance modes, but also provides a platform to demonstrate a Fabry–Pérot quasi-BIC laser by combining organic dye molecules with inorganic grating. Finite difference-time-domain (FDTD) numerical simulations have been performed to evaluate the performance of the aforementioned system with the results suggesting that a high-Q quasi-BIC mode ($Q > 10^4$) can be established by carefully optimizing the HCG structural parameters. Then, when the quasi-BIC mode spectrum overlaps with that of the gain material, a pronounced lasing action is obtained. More significantly, this quasi-BIC laser allows for a highly precise environment change detection through the reading of the emission wavelength shift. The achieved narrow linewidth (0.05 nm) combined with a large bulk sensitivity of 221 nm/RIU, results in a FOM of 4420 RIU^{-1}, which is approximately 20 times larger than typical passive sensors [27]. Therefore, our results suggest that the proposed quasi-BIC laser offers great potential for optical sensing of gases in low-concentration.

2 Resonator design and numerical model

2.1 Structure design

The schematic diagram of proposed double-HCG resonant structure is shown in Figure 1. The structure is designed to support a quasi-BIC at wavelength of 570 nm. The active region consists of 215 nm thick SiO_2 layer doped with Rhodamine 6G (R6G), as shown in Figure 1(a). A similar gain medium has been reported in a previous work [28]. The R6G layer is surrounded by Si_3N_4 stripes with a symmetric arrangement along z direction, and the refractive index of Si_3N_4 is 2.0. The HCG parameters are described by the thickness of grating layer T, filling factor (the grating width divided by the period) F and the period Λ. We consider the dimensions of whole device in x- and y-direction are infinite, as exhibited in Figure 1(b). The detail parameters of materials are shown in Table 1.

In the point of fabrication view, although there may exist several technical challenges, several experiments on

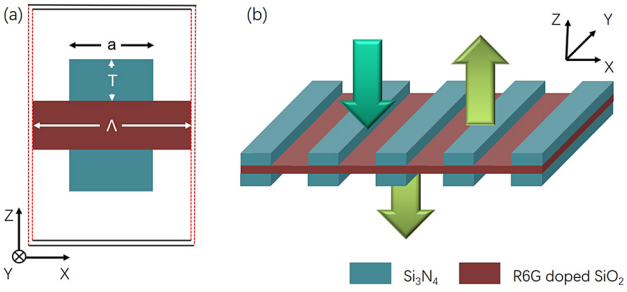

Figure 1: Schematic of proposed resonator based on HCGs: (a) single unit cell of two dimensional resonator; (b) whole structure with the organic R6G thin layer. The dark green downward arrow represents optical pump, the light green arrows on both sides of resonator are emitted light from the resonator.

Table 1: Material parameters.

Layer	Material	Refractive index	Thickness (nm)
Top HCG	Si_3N_4	2.0	230
Gain	R6G-doped SiO_2	1.46	215
Bottom HCG	Si_3N_4	2.0	230

the similar grating structure have been reported [29, 30]. A freestanding cascade grating fabrication technique, based on positive resist e-beam lithography (EBL) and ion coupling plasma, is supposed to be feasible to fabricate the designed structure. The SiO_2 layer doped with R6G can be made by using sol–gel technique, which is a suitable method for incorporating organic molecules into inorganic solid hosts. The low-temperature process involving the hydrolysis and condensation reactions of metal alkoxides enables us to dope different molecules with a poor thermal stability into coating films [31]. The fabrication process mainly includes thin film deposition and grating pattern. The Si_3N_4 thin film is uniformly coated with SiO_2 doped R6G sol solution, and then cover another Si_3N_4 thin film on the other side. The grating structures can be separately patterned on both sides by using EBL and ICP with CHF_3 gas [32]. A similar sandwiching structure consisting of two aluminum gratings and a Si_3N_4 membrane has been reported recently [33].

2.2 Theory and simulation

A semi-quantum framework is adopted to simulate the interaction between the electromagnetic fields and gain medium. The organic dye molecules in this work are well described as a four-energy-level system, and the population inversion is generated between the electronic level of L_2 state and L_1 state. As shown in Figure 2, which presents the population dynamics of the four relevant electronic levels of the molecule, such as the ground state, L_0, and the three excited states, L_1, L_2, and L_3. The molecular polarization given by spontaneous and stimulated transitions are described through the following equation [34]:

$$\frac{\mathrm{d}^2\vec{P}_{i,j}}{\mathrm{d}t^2} + \Delta\omega_{i,j}\frac{\mathrm{d}\vec{P}_{i,j}}{\mathrm{d}t} + \omega_{i,j}^2\vec{P}_{i,j} = \kappa_{(i,j)}\Delta N_{i,j}(t)\vec{E}(t) \quad (1)$$

where $\Delta\omega_{i,j}$ and $\omega_{i,j}$ are the bandwidth and frequency of the transition between states i and j, $\kappa_{i,j} = 6\pi\varepsilon_0 c^3/\left(\omega_{i,j}^2 \cdot \tau_{i,j}\right)$ [35], $\tau_{i,j}$ represents the lifetime of the spontaneous emission. $\Delta N_{i,j}(t)$ is the difference of population density between two energy states of the interest. $\vec{E}(t)$ is the total electric field, and can be calculated by solving the curl Maxwell equations [36]:

$$\nabla \times \vec{E}(t) = -\mu_0\frac{\partial\vec{H}(t)}{\mathrm{d}t}, \quad (2)$$

$$\nabla \times \vec{H}(t) = \varepsilon\frac{\partial\vec{E}(t)}{\partial t} + \frac{\partial(\vec{P}_{30}(t) + \vec{P}_{21}(t))}{\partial t} \quad (3)$$

In order to solve for the fields in a self-consistent fashion, it is necessary to couple the molecular polarization $\vec{P}_{i,j}$ to the electromagnetic fields via the rate equations of the four-level system describing the gain medium [37]. Such rate equations describe the time evolution of the energy states' population densities, and are given by Ref. [38]. The time evolution of each energy state density is described by their respective spontaneous decay processes $N_i/(\tau_{i,j})$ and stimulated processes $(\vec{E}(t) \cdot \mathrm{d}\vec{P}_{i,j}/\mathrm{d}t)$. The field involved in the rate equations is the total field and accounts for the effects of any local optical intensity on the dynamics of the population densities.

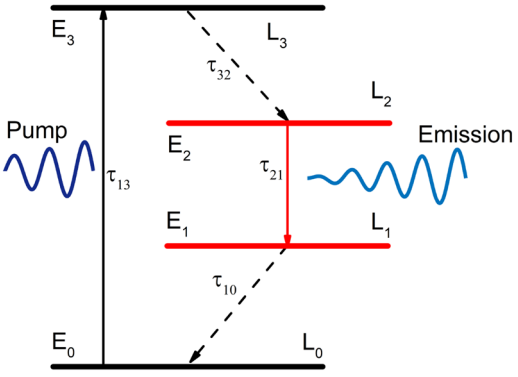

Figure 2: Energy level diagram and parameters used for modelling the dye molecules in FDTD simulations. The transition energies are $E_{30} = E_3 - E_0$ and $E_{21} = E_2 - E_1$. Since the transition from L_3 to L_2 is much faster than the transition from L_3 to L_0, the excitation quickly decay to L_2, leading to a population inversion for the transition from L_2 to L_1.

The FDTD method is adopted to solve the coupled equations. A plane wave in 4 ps pump pulse normally incident on the device along z-direction, as shown by the dark green downward arrow in Figure 1(b), and its center wavelength is $\lambda_P = 512$ nm. For the case of R6G-doped SiO_2, we set that the absorption transition: $\lambda_a = 512$ nm and $\Delta\lambda_a = 35$ nm; the emission transition: $\lambda_e = 570$ nm and $\Delta\lambda_e = 50$ nm; the concentration of dye molecule: $C = 1 \times 10^{19}$ cm^{-3}, which is comparable to the concentrations previously reported in the same material host [28]; and the lifetimes: $\tau_{32} = \tau_{10} = 5 \times 10^{-14}$s, $\tau_{30} = 1 \times 10^{-9}$ s, $\tau_{21} = 1.8 \times 10^{-9}$ s. Finally, the calculated emission cross section is around 3×10^{-16} cm^2, which is also consistent with the experimental report [39].

3 Bound states in the continuum and quasi-BIC lasing

3.1 BIC modes supported by the passive structure

First, the optical properties of single HCG layer are analyzed. To obtain a perfect mirror for light trapped in

a Fabry–pérot BIC system, we carry out FDTD simulations and calculate the structure's reflectance, for a normally incident plane wave polarized along the y-direction. Figure 3(a) illustrates the results of our simulations as a function of the wavelength and of the grating thickness, taking a grating filling factor $F = 0.5$. We observe two regions, which we refer to as the dual/multi-mode region (from $\lambda = 530$ to 700 nm) and the single-mode region ($\lambda > 700$ nm), as suggested by previous nomenclature [40]. For the single mode region, the grating operates in a longer wavelength regime, behaving like a quasi-uniform layer [17], so only Fabry–Pérot modes are supported in this wavelength range. On the other hand, in the dual/multi-modes region, the pattern is quite different, describing contrasting regions with high (> 99%) and low reflectance. In addition, we find the localized patterns do not change in an obvious manner when modify the filling factor F, instead, just an overall shifting to the longer wavelength. The reflectance spectrum shown in Figure 3(a) reveals that with a proper selection of the grating parameters (e.g., the thickness T, filling factor F, and period Λ), an ultra-high (> 99%) reflectivity over a spectral range is achievable (as shown by the double arrow line).

We proceed now to study the optical properties of the entire passive structure (SiO_2 layer sandwiched by the two HCGs) as a function of the main structural parameters. Figure 3(b) displays the reflectance spectra mapping as function of SiO_2 layer thickness, under the condition of $T = 230$ nm, $F = 0.50$, and $\Lambda = 530$ nm. We notice there are a series of discrete reflectance vanishing points at the SiO_2 layer thickness of 20, 210, 400, and 590 nm, corresponding to a periodical disappearance of resonance. These singular points break the high reflection continuum, showing the typical feature of Fabry–Pérot BIC. As mentioned before, an HCG layer possesses high reflectivity within a wide range, thus two HCGs layers with a symmetric alignment can make a Fabry–Pérot cavity. Therefore, BICs are formed when the distance between two HCG layers is tuned to make the round-trip phase shifts add up to an integer multiple of 2π [13]. Similar phenomenon was observed in a hybrid structure composed of a subwavelength grating layer and an un-patterned high-refractive-index cap layer [41]. However, the BIC nature of the modes was not identified. In addition, the high Q resonance in such a structure originates from the constructive interference of two Bloch modes in the grating layer, which is fundamentally different from the Fabry–Pérot BIC that exits in double gratings and stacked photonic crystal (PhC) slabs.

To obtain a quasi-BIC mode at wavelength of 566 nm that could be employed in a practical device, we slightly increase the thickness of SiO_2 layer by 5 nm. Figure 3(c) shows the band diagram of the designed structure, which is plotted by varying the angle of incidence (θ, from −25° to 25°) with respect to the z-axis. We observe symmetric patterns relative to the axis of $\theta = 0°$ (also Γ point), and the quasi-BIC mode at the position of mode 2, where is marked by the arrow and number '2', is successfully identified. This quasi-BIC mode exhibits a low dispersion near $\theta = 0°$ around 566 nm, suggesting a strong resonance in individual unit cell [42]. Apart from mode 2, we also find other BIC modes at $\theta = 0°$ (e.g., positions marked by '1' and '3') and 14.8° (e.g., position marked by '4'). Those BICs feature vanishing linewidths, suggesting a nonleaky state [4].

To further characterize the quasi-BIC at mode 2, we plot the field distribution profile in (x, z)-plane for this mode under the incident angle $\theta = 0°$, as shown in Figure 3(d). The E_y distribution of mode 2 over the (x, z)-plane shows a strong confinement within the cavity and a symmetric profile along z-direction. Due to the high reflectance of the HCGs and the sub-wavelength thickness of the SiO_2 layer, the first-order standing wave (i.e., one peak across the SiO_2 layer) is observed [43]. Typically, Fabry–Pérot BIC can be generated in systems with two identical resonances coupled to a single radiation channel [13]. Here, the round-trip phase shift between the two resonances in HCGs is

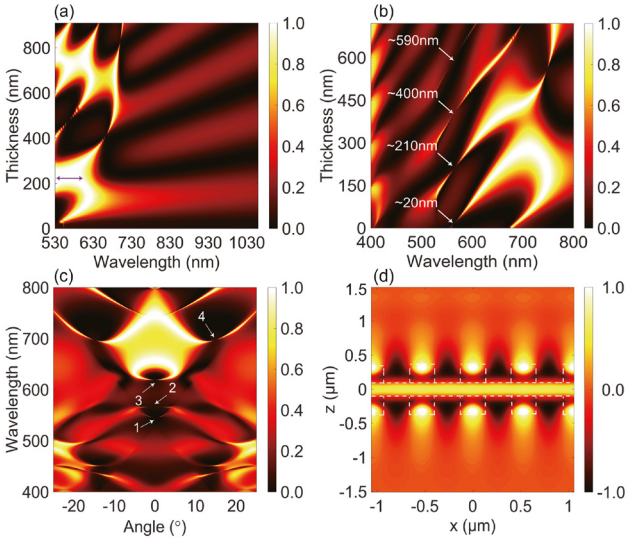

Figure 3: Reflectance spectra mapping and electric field distribution profile.
(a) Reflectance spectra mapping as a function of grating thickness when the filling factor $F = 0.50$; (b) reflectance spectra as a function of the thickness of SiO_2; (c) reflectance contour distribution of the architecture by sweeping the incident angle from −25° to 25°; (d) electric field distribution profiles within four periods corresponding to the places marked by '2'.

2π, thus the field is constructively interfered and trapped in the cavity while the resonant radiations from the HCGs interfere destructively out side of the cavity, which leads to the formation of Fabry–Pérot BIC.

3.2 Quasi-BIC lasing and characterization

To realize quasi-BIC lasing, we selected the grating parameters (T = 230 nm, F = 0.50, and Λ = 530 nm) which can provide the highest possible reflectivity (as marked in Figure 3), and the SiO_2 thickness is 215 nm. Then, R6G dye molecules are doped into SiO_2 thin layer to compensated the internal losses of resonator. As shown in Figure 1(b), the proposed sandwiched structure recalls conventional VCSELs, however, our design significantly reduces the cavity length. Figure 4(a) shows the gain spectrum of R6G (black curve), the spectrum of the cavity mode (blue curve) and typical lasing spectrum of resonator (red curve). Clearly, the R6G gain spectrum has a broad linewidth with its central region overlapping with the cavity mode peak, a feature guaranteeing a proper compensation of the cavity losses. Interestingly, the cavity mode shows the typical asymmetric line shape of a Fano resonance. This resonance is caused by the interference of radiative (bright) and nonradiative (dark) modes [44, 45]. For Si_3N_4-based HCG resonator, dark mode is associated with the Bragg scattering induced by HCG in the lateral direction, which results in a resonant mode with narrow bandwidth. On the other hand, the bright mode is associated with the weak Fabry–Pérot mode induced by the index difference in the vertical direction, which results in a mode with nearly flat-band spectrum. The interference of these two modes result in an asymmetric line shape of the spectrum [46, 47]. Moreover, this phenomenon could confine the optical mode in the structure well and result in a high Q factor, which is beneficial for the BIC laser operation with very narrow linewidth (red curve).

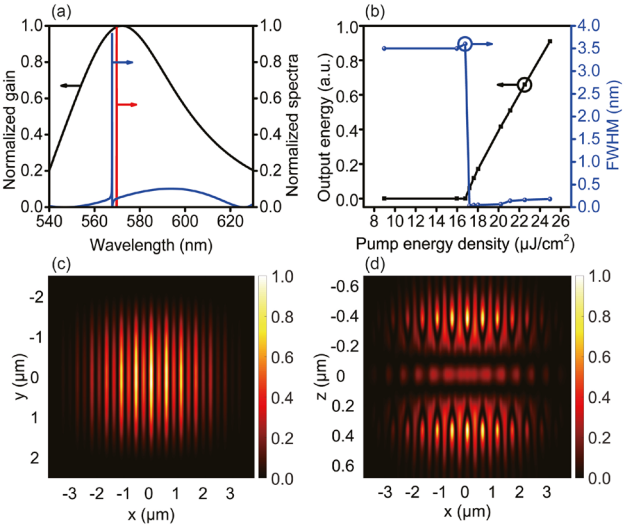

Figure 4: Lasing characterization results.
(a) Gain spectrum of R6G (black curve), cavity mode spectrum (blue curve), and typical emission spectrum of laser (red curve) operated above threshold; (b) input–output function curve (black) and spectrum linewidth changing as a function of input energy (blue); (c) near field intensity distribution of laser in (x, y) plane at z = 612.5 nm; (d) electric field intensity distribution in (x, z) plane at y = 0 nm. Both near fields are calculated at the peak laser emission wavelength, and the pump beam size in the simulation is 7.6 μm × 5.0 μm.

Figure 4(b) shows the detail characterizations of lasing behaviour. The black curve is the conventional plot of output power as a function of pump energy density, so we can estimate the threshold is around 17 μJ/cm^2, and the output power can reach to more than 40 μW when the pump is 25 μJ/cm^2, which is close to the power of practical device. The blue curve represents the corresponding optical spectrum linewidth (the full-width at half-maximum of the peak, FWHM) changing, the sharp narrowing of spectrum also indicates a coherence emission is achieved when the laser is operated above threshold. Both results are clear indications of lasing. We notice the linewidth is pump power modulated, and it becomes broader in far above threshold region. Such behavior has been reported in several experimental investigations on plasmonic laser systems [48, 49], and can be attributed to the dependence of refractive index on pump power.

Figure 4(c) and (d) are the electric field intensity distributions of resonator in (x, y) and (x, z) planes, respectively. When the resonator is operated above threshold, a large mode overlaps with the input pump contributing to a simple and efficient coupling of the input light, as suggested by the high intensity interfere fringes. In addition, the far field observation indicates a single mode lasing, which makes the laser device is more attractive. From the side view (Figure 4(d)), it is clear how the light is predominantly confined within the grating bars and there is exactly one intensity lobe within the interval of neighboring bars. In the middle, higher intensity stripe indicates the gain medium region, where we can find the vertical confinement of this device is much stronger than the confinement typically found in conventional DBRs-based vertical cavity emitting lasers. Since the double gratings provide the largest power reflectance, all diffraction orders disappear except the 0th order. In addition, the HCGs bring a higher effective refraction index and much higher than the surrounding

environment, leading to strong lateral confinement for the lateral modes.

4 Sensing function for gas detection

High-Q resonators with narrow resonance line widths and long photon storage time, have been considered as ideal candidates for sensors with enhanced detection sensitivity [50, 51]. Therefore, we carry out quantitative calculations of the quasi-BIC laser intrinsic sensitivity upon changes of the surrounding refractive index. We first reproduced a gas environment and immersed the resonator in a atmosphere of known refractive index value, then performing a refractive index change from 1.0000 to 1.0020. Figure 5(a) displays the full lasing spectra of the device versus variation of refractive index, where it is easily observe a shift of the emission wavelength towards a longer wavelengths, even though the refractive index increase step was just of the order of 5×10^{-4}. The inset exhibits the laser spectra upon change of the gas environment, where we notice

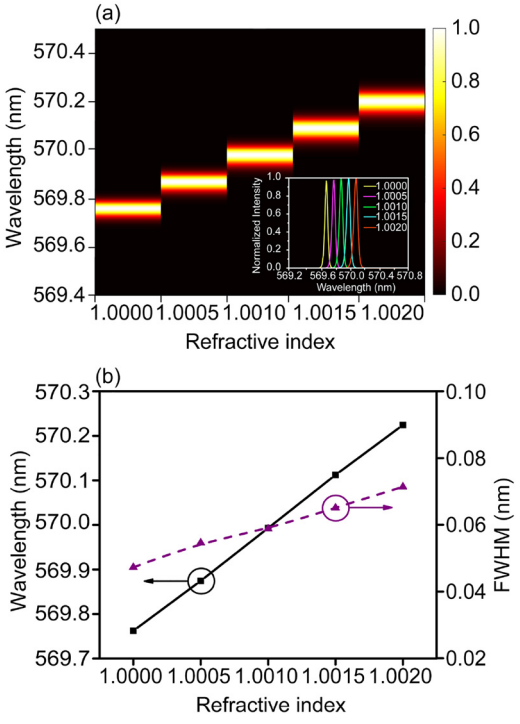

Figure 5: Sensing characterization.
(a) Mapping of emission wavelength shift with the variation of environment refractive index, inset: full lasing spectra for different refractive indexes; (b) linear relationship between emission wavelength shift and environment refractive index (black curve), and the corresponding spectrum linewidth changing with refractive index.

a single wavelength shifting without any other obvious changing. This also can be found from Figure 5(b), which presents the linear dependence of emission peaks on the refractive index (black curve), and the linewidth variation (dash curve). It is further confirmed that the change of refractive index results in only the shift of lasing wavelength without affecting the lasing state. This simple linear relationship between lasing wavelength shift and the variation of environment confirms the sensing capability of the proposed microlaser structure.

Specifically, the sensing performance of the device was evaluated by estimating the sensitivity (S_λ) and figure of merit (FOM_λ), which can be calculated through using the following formulas:

$$S_\lambda = \frac{\Delta\lambda}{\Delta n}, \tag{4}$$

$$\mathrm{FOM}_\lambda = \frac{S_\lambda}{\gamma} \tag{5}$$

where $\Delta\lambda$ represents the emission wavelength shifting, and Δn is the change of refractive index. γ is the emission spectrum linewidth measured at its full width at half maximum. FOM parameter is another important and more comprehensive benchmark to evaluate sensing performance [52, 53]. From the results in Figure 5(b), we calculated the S_λ and FOM_λ, which are 221 nm/RIU and 4420 RIU^{-1}, respectively. Very importantly, the achieved FOM value resulted much higher than the theoretical result for localized surface plasmon resonance sensors (~20) [54], PhC cavity [25], microring [55], and fiber Bragg grating sensors [56]. It is also comparable with that of state-of-the-art symmetry guided-mode resonance based sensors [52]. In addition, the organic gain enabled laser design leads to a coherent light source, which can either be detected at optical far field, or be easily coupled into fiber system. Thus, this flexible operation will facilitate the experimental measurements. In addition, the simple structure design will effectively reduce the cost of fabrication, making the sensor more appealing.

5 Conclusions

In conclusion, we have presented the design and numerical characterization of a compact quasi-BIC-laser based sensor for detecting of gas environment changing. The sensor is designed by using double Si_3N_4 HCG grating layers and organic R6G dye molecule doped SiO_2 layer located between the grating layers. The proposed unique hybrid design enables stimulated vertical emission from the organic gain medium embedded in the HCG stripes. Optimizations concerning HCGs and microcavity configuration

designed for a 570 nm resonant wavelength have been performed. Our design features a high-Q resonance, which enables a narrow-linewidth laser emission of 0.05 nm. Therefore, a pronounced BIC lasing behavior with narrow spectrum linewidth have been realized. The emitted light is close to the plane wave in air, which indicates a single lobe far field pattern for laser beam distribution. The sensing mechanism can be reasonably explained through the guided-mode resonance effect originated by constructive interference between the guided modes of the slab grating and the strong reflection modes. Finally, we also investigated the bulk sensing performance by inserting the device in some specific environment with different refractive index values, demonstrating remarkable sensitivity and figure of merit estimated equal to 221 nm/RIU and 4420 RIU^{-1}, respectively. Especially the figure of merit value outperforms recently reported GRM devices [52, 57] and other state-of-the-art passive sensors [25]. In view of these achievements, it is believed that this new platform could improve the current technology in remote gas sensing, e.g., warning from dangerous chemical gas.

Acknowledgments: We are grateful to Prof. Yang Li from Tsinghua University for useful discussions.
Author contribution: All the authors have accepted responsibility for the entire content of this submitted manuscript and approved submission.
Research funding: This work is supported in part by the National Natural Science Foundation of China (Grant No. 61804036, 61875051, 61801426), Zhejiang Province Natural Science Foundation (Grant No. LGJ20A040001, LR21F010002, Z20F010018), Federico Baur Endowed Chair in Nanotechnology, Fundamental Research Funds for the Central Universities and Zhejiang University Global Partnership Fund.
Conflict of interest statement: The authors declare no conflicts of interest regarding this article.

References

[1] S. Joseph, S. Sarkar, S. Khan, and J. Joseph, "Exploring the optical bound state in the continuum in a dielectric grating coupled plasmonic hybrid system," *Adv. Opt. Mater.*, vol. 9, p. 2001895, 2021.
[2] J. von Neumann and E. Wigner, "On the behavior of eigenvalues in adiabatic processes," *Phys. Z.*, vol. 30, p. 467, 1929.
[3] S. Han, L. Cong, Y. K. Srivastava, et al., "All dielectric active terahertz photonics driven by bound states in the continuum," *Adv. Mater.*, vol. 31, p. 1901921, 2019.
[4] C. Marinica, A. G. Borisov, and S. V. Shabanov, "Bound States in the continuum in photonics," *Phys. Rev. Lett.*, vol. 100, p. 183902, 2008.
[5] C. W. Hsu, B. Zhen, J. Lee, et al., "Observation of trapped light within the radiation continuum," *Nature*, vol. 499, pp. 188–191, 2013.
[6] T. Dong, J. Liang, S. Camayd-Munoz, et al., "Ultra-low-loss on-chip zero-index materials," *Light Sci. Appl.*, vol. 10, p. 10, 2021.
[7] H. Tang, C. DeVault, S. A. Camayd-Munoz, et al., "Low-loss zero-index materials," *Nano Lett.*, vol. 21, pp. 914–920, 2021.
[8] A. A. Lyapina, D. N. Maksimov, A. S. Pilipchuk, and A. F. Sadreev, "Bound states in the continuum in open acoustic resonators," *J. Fluid Mech.*, vol. 780, pp. 370–387, 2015.
[9] Y. X. Xiao, G. Ma, Z. Q. Zhang, and C. T. Chan, "Topological subspace-induced bound state in the continuum," *Phys. Rev. Lett.*, vol. 118, p. 166803, 2017.
[10] C. M. Linton and P. McIver, "Embedded trapped modes in water waves and acoustics," *Wave Motion*, vol. 45, pp. 16–29, 2007.
[11] C. W. Hsu, B. Zhen, A. D. Stone, J. D. Joannopoulos, and M. Soljacic, "Bound states in the continuum," *Nat. Rev. Mater.*, vol. 1, p. 16048, 2016.
[12] K. Koshelev, S. Kruk, E. Melik-Gaykazyan, et al., "Subwavelength dielectric resonators for nonlinear nanophotonics," *Science*, vol. 367, pp. 288–292, 2020.
[13] S. I. Azzam, V. M. Shalaev, A. Boltasseva, and A. V. Kildishev, "Formation of bound states in the continuum in hybrid plasmonic-photonic systems," *Phys. Rev. Lett.*, vol. 121, p. 253901, 2018.
[14] Z. F. Sadrieva, I. S. Sinev, K. L. Koshelev, et al., "Transition from optical bound states in the continuum to leaky resonances: role of substrate and roughness," *ACS Photonics*, vol. 4, pp. 723–727, 2017.
[15] A. Kodigala, T. Lepetit, Q. Gu, B. Bahari, Y. Fainman, and B. Kanté, "Lasing action from photonic bound states in continuum," *Nature*, vol. 541, pp. 196–199, 2017.
[16] S. T. Ha, Y. H. Fu, N. K. Emani, et al., "Directional lasing in resonant semiconductor nanoantenna arrays," *Nat. Nanotechnol.*, vol. 13, pp. 1042–1047, 2018.
[17] V. Karagodsky and C. J. Chang-Hasnain, "Physics of near-wavelength high contrast gratings," *Opt. Express*, vol. 20, pp. 10888–10895, 2012.
[18] S. G. Lee, S. H. Kim, and C. S. Kee, "Bound states in the continuum (BIC) accompanied by avoided crossings in leaky-mode photonic lattices," *Nanophotonics*, vol. 9, pp. 4373–4380, 2020.
[19] D. N. Maksimov, V. S. Gerasimov, S. Romano, and S. P. Polyutov, "Refractive index sensing with optical bound states in the continuum," *Opt. Express*, vol. 28, pp. 38907–38916, 2020.
[20] S. Romano, G. Zito, S. Torino, et al., "Label-free sensing of ultralow-weight molecules with all-dielectric metasurfaces supporting bound states in the continuum," *Photon. Res.*, vol. 6, no. 7, pp. 726–733, 2018.
[21] N. Bosio, H. Šípová-Jungová, N. O. Länk, T. J. Antosiewicz, R. Verre, and M. Käll, "Plasmonic versus all-dielectric nanoantennas for refractometric sensing: a direct comparison," *ACS Photonics*, vol. 6, pp. 1556–1564, 2019.
[22] R. M. Ma, S. Ota, Y. Li, S. Yang, and X. Zhang, "Explosives detection in a lasing plasmon nanocavity," *Nat. Nanotechnol.*, vol. 9, pp. 600–604, 2014.

[23] J. Sun, T. Wang, Z. Jafari, et al., "High-Q plasmonic crystal laser for ultra-sensitive biomolecule detection," *IEEE J. Sel. Top. Quant. Electron.*, vol. 27, pp. 1–7, 2021.
[24] F. Yesilkoy, E. R. Arvelo, Y. Jahani, et al., "Ultrasensitive hyperspectral imaging and biodetection enabled by dielectric metasurfaces," *Nat. Photonics*, vol. 13, no. 6, pp. 390–396, 2019.
[25] Y. Liu, S. Wang, D. Zhao, W. Zhou, and Y. Sun, "High quality factor photonic crystal filter at k ≈ 0 and its application for refractive index sensing," *Opt. Express*, vol. 25, pp. 10536–10545, 2017.
[26] C. Huang, C. Zhang, S. Xiao, et al., "Ultrafast control of vortex microlasers," *Science*, vol. 367, pp. 1018–1021, 2020.
[27] M. Maleki, M. Mehran, and A. Mokhtari, "Design of a near-infrared plasmonic gas sensor based on graphene nanogratings," *J. Opt. Soc. Am. B*, vol. 37, pp. 3478–3486, 2020.
[28] A. Anedda, C. M. Carbonaro, F. Clemente, et al., "Rhodamine 6G-SiO2 hybrids: a photoluminescence study," *J. Non-Cryst. Solids*, vol. 351, pp. 1850–1854, 2005.
[29] A. E. Hollowell, C. L. Arrington, P. Finnegan, et al., "Double sided grating fabrication for high energy X-ray phase contrast imaging," *Mater. Sci. Semicond. Process.*, vol. 92, pp. 86–90, 2019.
[30] M. Athanasiou, R. M. Smith, S. Ghataora, and T. Wang, "Polarized white light from hybrid organic/III-nitrides grating structures," *Sci. Rep.*, vol. 7, p. 39677, 2017.
[31] H. Yanagi, T. Hishiki, T. Tobitani, A. Otomo, and S. Mashiko, "Thin film lasing from a dye-doped silicartitania composite," *Chem. Phys. Lett.*, vol. 292, pp. 332–338, 1998.
[32] J. Hong, A. M. Spring, F. Qiu, and S. Yokoyama, "A high efficiency silicon nitride waveguide grating coupler with a multilayer bottom reflector," *Sci. Rep.*, vol. 9, p. 12988, 2019.
[33] Y. Liang, N. Ruan, S. Zhang, Z. Yu, and T. Xu, "Experimental investigation of extraordinary optical behaviors in a freestanding plasmonic cascade grating at visible frequency," *Opt. Express*, vol. 26, pp. 3271–3276, 2018.
[34] X. L. Zhong and Z. Y. Li, "All-analytical semiclassical theory of spaser performance in a plasmonic nanocavity," *Phys. Rev. B*, vol. 88, p. 085101, 2013.
[35] K. Wang, H. Qian, Z. Liu, and P. K. L. Yu, "Second-order nonlinear susceptibility enhancement in gallium nitride nanowires," *Prog. Electromagn. Res.*, vol. 168, pp. 25–30, 2020.
[36] M. Dridi and G. C. Schatz, "Model for describing plasmon-enhanced lasers that combines rate equations with finite-difference time-domain," *J. Opt. Soc. Am. B*, vol. 30, pp. 2791–2797, 2013.
[37] D. J. Trivedi, D. Wang, T. W. Odom, and G. C. Schatz, "Model for describing plasmonic nanolasers using Maxwell-Liouville equations with finite-difference time-domain calculations," *Phys. Rev. A*, vol. 96, p. 053825, 2017.
[38] W. Zhou, M. Dridi, J. Y. Suh, et al., "Lasing action in strongly coupled plasmonic nanocavity arrays," *Nat. Nanotechnol.*, vol. 8, pp. 1–6, 2013.
[39] T. Grossmann, S. Schleede, M. Hauser, et al., "Low-threshold conical microcavity dye lasers," *Appl. Phys. Lett.*, vol. 97, p. 063304, 2010.
[40] C. J. Chang-Hasnain and W. Yang, "High-contrast gratings for integrated optoelectronics," *Adv. Opt. Photon.*, vol. 37, pp. 379–440, 2012.
[41] A. Taghizadeh, J. Mørk, and I.-S. Chung, "Ultracompact resonator with high quality-factor based on a hybrid grating structure," *Opt. Express*, vol. 23, pp. 14913–14921, 2015.
[42] A. Taghizadeh and I. I. Chung, "Quasi bound states in the continuum with few unit cells of photonic crystal slab," *Appl. Phys. Lett.*, vol. 111, p. 031114, 2017.
[43] J. M. Fitzgerald, S. K. Manjeshwar, W. Wieczorek, and P. Tassin, "Cavity optomechanics with photonic bound states in the continuum," *Phys. Rev. Res.*, vol. 3, p. 013131, 2021.
[44] M. F. Limonov, M. V. Rybin, A. N. Poddubny, and Y. S. Kivshar, "Fano resonances in photonics," *Nat. Photonics*, vol. 11, pp. 543–554, 2017.
[45] H. Heo, S. Lee, and S. Kim, "Tailoring Fano resonance for flat-top broadband reflectors based on single guided-mode resonance," *J. Lightwave Technol.*, vol. 37, pp. 4244–4250, 2019.
[46] T. T. Wu, S. H. Wu, T. C. Lu, and S. C. Wang, "GaN-based high contrast grating surface-emitting lasers," *Appl. Phys. Lett.*, vol. 102, p. 081111, 2013.
[47] Y. Zhou, M. C. Y. Huang, C. Chase, et al., "High-index-contrast grating (HCG) and its applications in optoelectronic devices," *IEEE J. Sel. Top. Quant. Electron.*, vol. 15, pp. 1485–1499, 2009.
[48] A. Yang, T. B. Hoang, M. Dridi, et al., "Real-time tunable lasing from plasmonic nanocavity arrays," *Nat. Commun.*, vol. 6, p. 6939, 2015.
[49] W. Zhu, T. Xu, H. Wang, et al., "Surface plasmon polariton laser based on a metallic trench Fabry-Perot resonator," *Sci. Adv.*, vol. 3, p. e1700909, 2017.
[50] D. K. Armani, T. J. Kippenberg, S. M. Spillane, and K. J. Vahala, "Ultra-high-q toroid microcavity on a chip," *Nature*, vol. 421, pp. 925–928, 2003.
[51] J. Zhu, S. K. Ozdemir, Y. F. Xiao, et al., "On-chip single nanoparticle detection and sizing by mode splitting in an ultrahigh-Q microresonator," *Nat. Photonics*, vol. 4, pp. 46–49, 2010.
[52] Y. Zhou, X. Li, S. Li, et al., "Symmetric guided-mode resonance sensors in aqueous media with ultrahigh figure of merit," *Opt. Express*, vol. 27, pp. 34788–34802, 2019.
[53] Q. L. Huang, J. Peh, P. J. Hergenrother, and B. T. Cunningham, "Porous photonic crystal external cavity laser biosensor," *Appl. Phys. Lett.*, vol. 109, p. 071103, 2016.
[54] J. M. Bingham, J. N. Anker, L. E. Kreno, and R. P. Van Duyne, "Gas sensing with high-resolution localized surface plasmon resonance spectroscopy," *J. Am. Chem. Soc.*, vol. 132, pp. 17358–17359, 2010.
[55] C. Chung-Yen, W. Fung, and L. J. Guo, "Polymer microring resonators for biochemical sensing applications," *IEEE J. Sel. Top. Quant. Electron.*, vol. 12, pp. 134–142, 2006.
[56] X. Li, S. Liang, Y. Zhang, et al., "Novel refractive index sensor based on fiber Bragg grating in nano-bore optical fiber," *Opt. Quant. Electron.*, vol. 51, p. 117, 2019.
[57] Y. H. Wan, N. A. Krueger, C. R. Ocier, P. Su, P. V. Braun, and B. T. Cunningham, "Resonant mode engineering of photonic crystal sensors clad with ultralow refractive index porous silicon dioxide," *Adv. Opt. Mater.*, vol. 5, p. 1700605, 2017.